

Novel analysis technique for measuring edge density fluctuation profiles with reflectometry in the Large Helical Device

A. J. Creely, K. Ida, M. Yoshinuma, T. Tokuzawa, T. Tsujimura, T. Akiyama, R. Sakamoto, M. Emoto, K. Tanaka, and C. A. Michael

Citation: [Review of Scientific Instruments](#) **88**, 073509 (2017); doi: 10.1063/1.4993437

View online: <https://doi.org/10.1063/1.4993437>

View Table of Contents: <http://aip.scitation.org/toc/rsi/88/7>

Published by the [American Institute of Physics](#)

Articles you may be interested in

[An eight-channel Doppler backscattering system in the experimental advanced superconducting tokamak](#)
[Review of Scientific Instruments](#) **88**, 073504 (2017); 10.1063/1.4991855

[A novel approach to estimating the Doppler shift frequency from quadrature mixer output](#)
[Review of Scientific Instruments](#) **88**, 073503 (2017); 10.1063/1.4991018

[Correlation electron cyclotron emission diagnostic in TCV](#)
[Review of Scientific Instruments](#) **88**, 083506 (2017); 10.1063/1.4997075

[Extensions to the charge exchange recombination spectroscopy diagnostic suite at ASDEX Upgrade](#)
[Review of Scientific Instruments](#) **88**, 073508 (2017); 10.1063/1.4993131

[Linear servomotor probe drive system with real-time self-adaptive position control for the Alcator C-Mod tokamak](#)
[Review of Scientific Instruments](#) **88**, 073501 (2017); 10.1063/1.4990043

[Validation of nonlinear gyrokinetic simulations of L- and I-mode plasmas on Alcator C-Mod](#)
[Physics of Plasmas](#) **24**, 056104 (2017); 10.1063/1.4977466



Nanopositioning Systems Micropositioning AFM & SPM Single molecule imaging

Novel analysis technique for measuring edge density fluctuation profiles with reflectometry in the Large Helical Device

A. J. Creely,^{1,a)} K. Ida,² M. Yoshinuma,² T. Tokuzawa,² T. Tsujimura,² T. Akiyama,² R. Sakamoto,² M. Emoto,² K. Tanaka,² and C. A. Michael³

¹MIT Plasma Science and Fusion Center, Cambridge, Massachusetts 02139, USA

²National Institute for Fusion Science, Toki, Gifu, Japan

³Plasma Research Lab, Australian National University, Canberra, Australia

(Received 15 March 2017; accepted 28 June 2017; published online 19 July 2017)

A new method for measuring density fluctuation profiles near the edge of plasmas in the Large Helical Device (LHD) has been developed utilizing reflectometry combined with pellet-induced fast density scans. Reflectometer cutoff location was calculated by proportionally scaling the cutoff location calculated with fast far infrared laser interferometer (FIR) density profiles to match the slower time resolution results of the ray-tracing code LHD-GAUSS. Plasma velocity profile peaks generated with this reflectometer mapping were checked against velocity measurements made with charge exchange spectroscopy (CXS) and were found to agree within experimental uncertainty once diagnostic differences were accounted for. Measured density fluctuation profiles were found to peak strongly near the edge of the plasma, as is the case in most tokamaks. These measurements can be used in the future to inform inversion methods of phase contrast imaging (PCI) measurements. This result was confirmed with both a fixed frequency reflectometer and calibrated data from a multi-frequency comb reflectometer, and this method was applied successfully to a series of discharges. The full width at half maximum of the turbulence layer near the edge of the plasma was found to be only 1.5–3 cm on a series of LHD discharges, less than 5% of the normalized minor radius. *Published by AIP Publishing.* [<http://dx.doi.org/10.1063/1.4993437>]

I. INTRODUCTION

Accurate measurements of density fluctuations in fusion plasmas are a key component in better understanding transport via drift wave turbulence. These measurements can be made with a variety of plasma diagnostics, including beam emission spectroscopy (BES),¹ phase contrast imaging (PCI),² and reflectometry.^{3–5} In tokamaks, where density fluctuation profiles have been studied extensively, it has generally been observed that density fluctuations increase sharply toward the edge of the plasma (see Refs. 6–11 for some examples).

This sharp increase in edge fluctuations may be due to a variety of causes. While the absolute edge density and temperature are lower than in the core, the gradients tend to be much higher, which tends to increase turbulence drive terms that go as the gradient normalized by the value.¹² In addition, there is a very sharp increase in the q profile and thus a very rapid shift in the magnetic configuration. It is possible that this change in magnetic configuration, and specifically the magnetic shear, also plays a role in the formation of edge turbulence.

In order to investigate the role of magnetic geometry in the formation of these edge fluctuations, it is important to measure these fluctuations on devices with a variety of magnetic geometries. This motivates the measurement of fluctuations in a helical device, such as the Large Helical Device (LHD).^{13,14}

There are few experimental measurements of density fluctuation profiles in helical devices. Many local measurements of

fluctuations at a single location have been made, but measurements on ATF,¹⁵ TJ-II,^{16,17} and Wendelstein 7AS¹⁸ are some of the few examples of full edge density fluctuation profile measurements on stellarators.

Previous work on LHD using inverted PCI measurements showed that the peaking of the density fluctuation profile depended heavily on the method of inversion^{19–22} and that some inversions led to profiles that peaked much further in radially than is seen in typical tokamak measurements. The PCI diagnostic is also susceptible to systematic errors due to optical misalignment, which may impact the measured location of the fluctuation profile peak.²¹

In order to further investigate these phenomena and avoid the use of inversions, this work develops a new analysis technique to measure the density fluctuation profile near the edge of LHD plasmas using local measurements with a reflectometer. Since reflectometers measure fluctuations only at one radial location, profile measurements are accomplished by scanning the reflectometer cutoff location via the fast density rise and fall following a pellet injection. This new analysis technique will enable the comparison of fluctuation profiles measured on LHD to those measured on tokamaks and other stellarators as well as informing future PCI inversions and systematic error correction on LHD.

Section II of this paper describes the various diagnostics and codes used in this study. Section III describes the analysis methods required to accurately map the reflectometer cutoff location and extract the fluctuation profile from the time signal. Section IV presents the fluctuation profiles measured with this new technique and gives evidence that the process is indeed

a) acreely@mit.edu

measuring spatial, rather than temporal, changes in density fluctuations. Section V presents conclusions and comparisons to past work, and motivates future work.

II. EXPERIMENTAL SETUP

Doppler reflectometry (or Doppler back-scattering) is widely used to measure turbulent flow velocity and amplitude in fusion plasmas.^{3–5}

Two types of Doppler reflectometers have been installed in LHD: a frequency-hopping system²³ and a multi-channel frequency comb system.²⁴ The frequency-hopping system is installed at the 9-O toroidal port (referred to as the “9-O” reflectometer) and typically set to 30.0 GHz, while the comb system is installed at the 3-O port (referred to as the “comb” reflectometer) and operates with frequencies of 27.7, 29.0, 30.5, 32.0, 33.3, 34.8, 37.0, and 38.3 GHz. These reflectometers measure turbulent electron density fluctuation perpendicular wave numbers of up to 15 cm^{-1} .^{5,24} These diagnostics measure density fluctuations with a k-spectrum width of approximately 2 cm^{-1} .⁵ Both of these reflectometers use bi-static antennae, separated vertically, not toroidally.

The simplest estimates of the reflectometer cutoff location are based solely on the cold plasma treatment of the density profiles (the location where the plasma frequency is equal to the launched wave frequency). Typically, however, a density profile alone is not sufficient to determine the exact reflectometer cutoff location since the complexities of the wave propagation in the plasma necessitate ray tracing codes.^{25,26}

A more accurate description of the measurement location is provided by ray tracing codes, which employ a variety of models for the plasma index of refraction. This study used the 3D ray tracing code LHD-GAUSS, which was recently upgraded and applied to electron cyclotron heating experiments in LHD.^{25,26} The code calculates ray trajectories of traveling probe waves by solving the eikonal equation under the WKB approximation. The propagation of each ray is based on the model of geometric optics with the cold plasma dispersion relation, where the electron density profile is provided by 3D equilibrium mapping of Thomson scattering measurements.²⁷ For the equilibrium electron density profiles, this study makes use of both Thomson scattering²⁸ and far infrared laser interferometer (FIR)²⁹ measurements.

Figure 1 shows an example of the reflectometer ray trajectory calculated with LHD-GAUSS. The observation position is determined by the reflection position of the ray trajectory. In this study, both reflectometers (the 9-O and the comb reflectometers) operated in the ordinary mode (O-mode) polarization. 3D results from the LHD-GAUSS code reveal that misalignment between the launched and received reflectometer beams due to toroidal displacement of the back-scattered beam is negligible (a few percent) compared to other uncertainties in these measurements, which are discussed below.

In addition to measurements with Doppler reflectometry, radial profiles of poloidal rotation velocity are measured with poloidal charge exchange spectroscopy (CXS), using recombination emission from fully ionized carbon and the hydrogen neutral beam.^{30,31} The diagnostic has two poloidal views, one

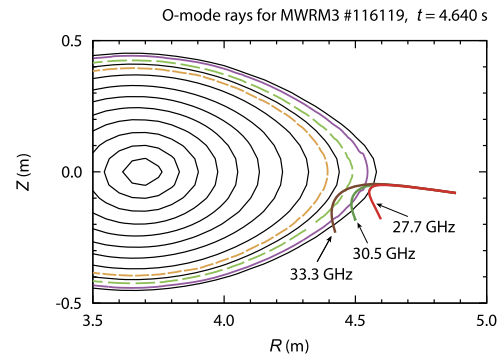


FIG. 1. Examples of ray trajectories calculated by the *LHD-GAUSS* code in a horizontal plasma cross section. The thick solid lines indicate the center rays of the probing beams, with frequencies of 27.7, 30.5, and 33.3 GHz. The thinner and dashed lines are the nominal cutoff densities, had ray tracing not been used. Ray tracing shows reflection before the nominal cutoff density.

upward and one downward. The spatial pitch of the poloidal lines of sight at the mid-plane is 9 mm in r_{eff} (13 mm in major radius), near the plasma edge. Since the poloidal velocity is derived from the difference in Doppler shift between the upward and downward views using three nearby channels, the effective spatial resolution is approximately 3 cm.

Section III describes how these diagnostics are used in a new analysis technique that measures radial density fluctuation profiles near the plasma edge.

III. ANALYSIS METHODS

A multi-step analysis process is required to extract the fluctuation profile from the raw reflectometer data. While each of these steps will be described in more detail later in this section, a brief summary is given here.

First, in order to determine the reflection location of the reflectometer with good time resolution, inverted FIR data were used to fit density profiles at 1 ms intervals. This was then checked against slower resolution Thomson scattering data as appropriate.

The 3D ray tracing code LHD-GAUSS is needed to determine the exact reflectometer cutoff location, as discussed in Sec. II. Running this code at every time slice, however, tends to be prohibitively slow, and so a faster method was desired. As a fast estimate of the cutoff location, the simplistic calculation based purely on the reflectometer frequency and density profile was redone with a cutoff density that was scaled by some constant factor, which was then checked against ray tracing results at appropriate time intervals to determine the appropriate scaling factor. The velocity profiles measured using this initial estimate and the density scan induced by the pellet injection (which radially scanned the cutoff location) were then checked against the velocity profile measured with charge exchange in order to further confirm the validity of this scaling method.

Once the cutoff density scaling has been determined using the ray tracing and velocity profile checks, the fluctuation profiles can be mapped with a more reliable cutoff location. The peak of the edge fluctuations is then used to calibrate the comb channels to the 9-O reflectometer, as these channels all have different arbitrary units and are not pre-calibrated to

one another. Once calibrated, the comb and 9-O reflectometers can be used to map out fluctuation profiles even in periods of constant density.

A. Profile fitting and reflectometer cutoff calculation

The first step of the fluctuation profile mapping process is the density profile fitting and cutoff location calculation. The reflectometer cutoff location must be calculated on a very fast time scale in order to resolve the fast density profile scan caused by the pellet injection. The FIR diagnostic has a very high time resolution (1 ms as it is set up) but a low spatial resolution, while Thomson scattering has a high spatial resolution but a slow time resolution (33 ms). For the purposes of this study, the fast FIR profiles were used and were then checked against the slower Thomson profiles to ensure consistency.

FIR is inherently a line-integrated diagnostic, so the first step involved a standard inversion of the FIR line-integrated data to achieve a density profile.²⁹ While there are relatively few spatial data points, a simple spline fit generated a straightforward profile. This profile fit is shown in Fig. 2. The spline-fit FIR profile was checked against the profile measured with Thomson scattering at time points where the Thomson data were taken. While there are small differences between the two profiles (such as the area around $r_{eff} = 0.5$ m), the two diagnostics generally agree quite well near the edge, which increases our confidence in the accuracy of the FIR profiles.

As a first cut, the reflectometer cutoff location was then calculated as the location where the density first reached the point where the plasma frequency was equal to the reflectometer launch frequency. The time evolution of the cutoff location after the pellet injection is shown by the red trace in Fig. 3. The other traces on this plot are discussed below. While obviously omitting all of the complexities of the reflectometer ray propagation, this method allows very fast calculation of the cutoff location at every 1 ms time slice, without running full ray tracing codes. In order to maintain this fast operation, while making use of more accurate ray tracing codes, the cutoff density calculated directly from the density

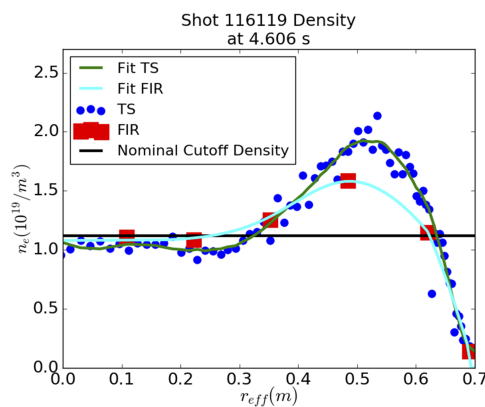


FIG. 2. Density profiles measured with Thomson scattering and FIR. Thomson data are smoothed with a Savitzky-Golay filter, and FIR data are spline fit. Also plotted is the cutoff density corresponding to the 9-O reflectometer launch frequency. FIR has low spatial, but high time, resolution. The fit agrees well with Thomson data near the reflectometer cutoff density.

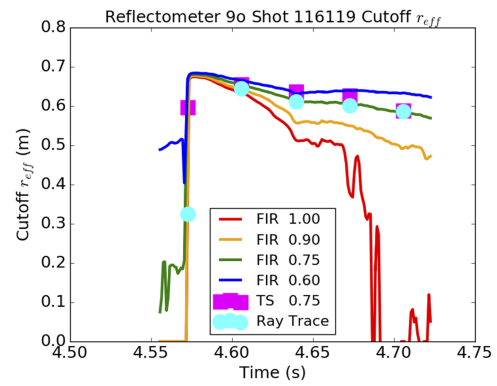


FIG. 3. 9-O reflectometer cutoff location calculated via scaled cutoff densities and FIR and Thomson density profiles, checked against ray tracing results. FIR cutoff density scalings of 1.00 (unscaled), 0.90, 0.75, and 0.60 are shown in various colors, along with a Thomson scaling of 0.75 and ray tracing calculations. A cutoff density scaling of 0.75 for both FIR (green line) and Thomson (magenta squares) agrees most closely with ray tracing results (cyan circles).

profiles was scaled by some constant factor until the cutoff location calculated by this simple method agreed with ray tracing results at sample time slices. This process is described in Sec. III B.

B. Scaling of cutoff density to match ray tracing cutoff and CXS velocity profiles

Once the density profiles have been fit and the initial calculation of the cutoff location has been completed, one can compare the cutoff location to the results of ray tracing codes in order to determine an appropriate scaling for the cutoff density. These results can then be checked by comparing the velocity profiles measured with the mapped cutoff to those measured by CXS.

Figure 3 shows the comparison of ray tracing output with the cutoff locations calculated from FIR density profiles with different cutoff density scalings ($n_{cutoff} = Scaling \cdot n_{cutoff,1.00}$). Ray tracing was run every 33 ms, while the FIR profiles were fit every 1 ms. The different colors represent different cutoff density scalings (the factor by which the cutoff density is multiplied). For this particular shot, a density cutoff scaling of approximately 0.75 achieves the best agreement with ray tracing results. While this example includes only one shot, it was observed that a scaling of between 0.7 and 0.8 worked best for most of the shots considered in this study. Figure 3 also shows a comparison with the calculations from Thomson profiles at the Thomson measurement times, also with a scaling of 0.75. The FIR and Thomson data with a scaling of 0.75 agree quite nicely both with each other and with the ray tracing calculation.

As an additional check of the accuracy of the reflectometer cutoff location, the velocity profile measured from the mapped cutoff location is now compared to the profile measured by CXS.

As discussed before, the density scan induced by a pellet injection can be used to scan the reflectometer cutoff location, and thus map out a profile of velocity and fluctuations. As the pellet enters the plasma, the density transiently increases and then decreases. This fast change in the density profile subsequently shifts the reflectometer cutoff location outward

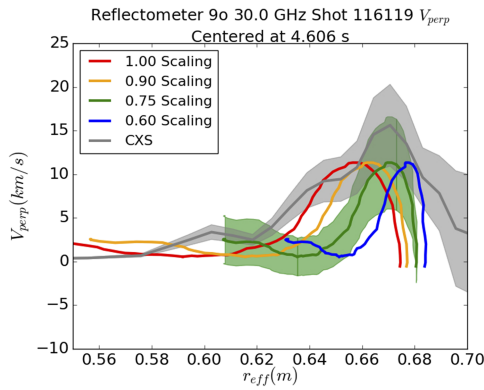


FIG. 4. Perpendicular velocity profile measurements from the 9-O reflectometer and CXS. Different colors represent different scalings for the cutoff density used to calculate the cutoff location on FIR density profiles. Diagnostic uncertainty is shown for the CXS data as the shaded grey region and for one scaling of the reflectometer data in shaded green. Closest agreement for the peak of the velocity profile measured with reflectometry and CXS is found for a cutoff scaling of 0.75.

and then back inward. One can then back out the velocity profile by mapping the measured velocity to the location at which it was measured.

The velocity profiles mapped from a variety of cutoff scalings are shown in Fig. 4. It should be noted that this comparison is intended *only* to confirm the reflectometer cutoff scaling factor, by comparing the peak of the velocity profile. It is *not* intended as a detailed comparison of velocity measurements in general by these two different diagnostics. See Ref. 3 for a further discussion of such comparisons.

Once again, it is clear that a scaling of approximately 0.75 generates the best agreement with the location and shape of the profile measured with CXS. The maximum magnitude differs by approximately 30%, while the overall width is very similar. The peaks of the two diagnostics agree within uncertainty.

There are a number of possible causes for this slight discrepancy. First, the wave number calculation for the reflectometer has an uncertainty of approximately 20%, primarily associated with the finite beam width, which is included in the uncertainty plotted above. In addition, the velocity measured with the reflectometer is the sum of the ExB velocity and the drift wave velocity, which is approximately -2 km/s for the axes shown on the plot (the electron diamagnetic direction). This slight discrepancy does not alter the assessment that the scaling of 0.75 agrees most closely with the CXS measurements. As stated above, detailed comparisons of reflectometer and CXS velocity measurements are beyond the scope of this paper.

One method of estimating the uncertainty associated with the cutoff mapping procedure involves varying the cutoff scaling and checking agreement with ray tracing within the ray tracing uncertainties. One can then use different scalings to map the measured velocity profile and check agreement with the CXS data. These methods both give an uncertainty of approximately ± 0.05 in the cutoff scaling. This uncertainty in the cutoff scaling is used to estimate the radial uncertainty shown in Figs. 5, 8, and 9.

As is expected, the smaller r_{eff} side of the profile seems to be more accurate than the larger r_{eff} side (core rather than

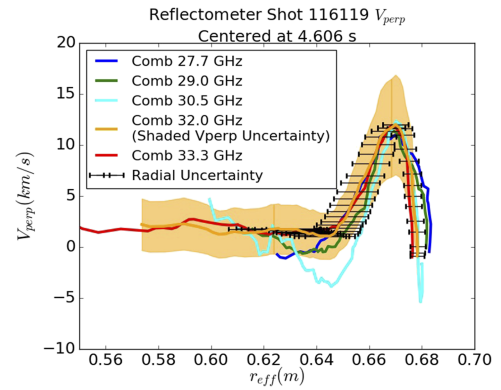


FIG. 5. Perpendicular velocity profiles measured with five channels of the comb reflectometer. A cutoff density scaling of 0.75 was used. Calibrated to the 9-O measurement. Representative uncertainty shown for the 32.0 GHz channel (velocity in shaded orange, radial as black error bars). Once calibrated, most channels agree within error bars.

scrape-off-layer) since the reflectometer measurements will be much less reliable outside of the last closed flux surface.

The general agreement in the profile peak shape and location indicates that the pellet-induced density scans allow accurate velocity profile measurements with the reflectometer and that the same method can likely be applied to density fluctuation measurements.

C. Calibration of comb reflectometer

In addition to using the density scan to compare to CXS in order to determine the appropriate cutoff density scaling, this scan can also be used to calibrate the multi-channel comb reflectometer against the single channel 9-O reflectometer. The 9-O reflectometer velocity measurements are calibrated to measure in km/s directly. The comb reflectometer, however, measures velocity in arbitrary units, which are also different for each channel. This means that without some type of cross-calibration, channels cannot be compared to one another or to the 9-O reflectometer.

The pellet-induced density scan can be used for just such a calibration. The profiles measured by all of the comb channels can be plotted on top of the 9-O profile and then calibrated such that the profiles agree as closely as possible. The same cutoff density scaling as for the 9-O reflectometer is used. Figure 5 shows the calibrated comb channels. Three comb channels were not operational in this shot and are therefore omitted from the figure. These profiles also agree quite closely with that measured with the 9-O reflectometer, shown in Fig. 4.

Once this calibration has been completed, one can then compare the different channels directly at other times in the shot. This enables profile measurements even during time periods with constant density.

More importantly, a similar procedure can be applied to the fluctuation profiles, described in Sec. IV, which allows measurement of fluctuation profiles at all times in the shot.

IV. DENSITY FLUCTUATION PROFILES

Once the reflectometer cutoff location has been calculated and scaled appropriately, and the comb reflectometer has been

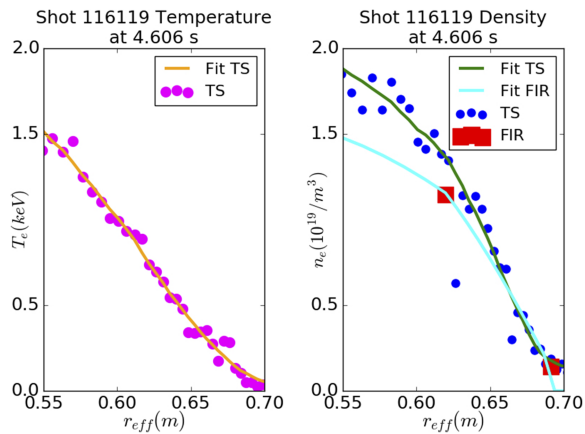


FIG. 6. Edge temperature and density profiles for one shot analyzed in this study. Raw data (symbols) and fits (lines) both shown.

calibrated to the 9-O reflectometer, one can use the pellet-induced density scan to measure the density fluctuation profiles in the same manner as the velocity profiles.

As reference, the temperature and density profiles in one plasma for which the fluctuations were measured are shown in Fig. 6.

A. Separation of fluctuation changes due to pellet and due to density scan

One possible complication of measuring a density fluctuation profile with a pellet injection-induced density scan is that the pellet injection itself causes some changes in the density fluctuations. This subsection will separate out these effects.

As discussed throughout this paper, the reflectometer location moves as the density changes, which possibly complicates the ability to separate spatial and temporal changes in fluctuations. PCI chords, however, do not move in space and will only measure changes in fluctuations over time. The PCI will therefore measure directly the temporal changes in fluctuations due to the pellet injection, without any change in location. One can then compare the time history of fluctuations measured with PCI and with the moving reflectometer channel in order to separate out the spatial and temporal dependence of the reflectometer measurements.

As with CXS, this comparison is *not* intended as a direct comparison of these two diagnostics, especially since they measure different wavenumber spectra, and is only intended as evidence that the fluctuation profiles measured in this section are due to the movement of the cutoff location of the reflectometer, not due to the pellet itself.

Time histories of fluctuations measured by one PCI channel which samples both edge and core (50-150 kHz) and the 9-O reflectometer (30-150 kHz) are shown in Fig. 7. The pellet is injected at around 4.56 s and causes a sharp rise in measured fluctuations on both the PCI and the reflectometer. This feature is highlighted in red and quickly decays away as the pellet-induced fluctuations dissipate. Then, starting at around 4.58 s, there is another feature on the reflectometer, highlighted in blue, that is entirely absent on the PCI. Since this feature is not observed on PCI, there is strong evidence that it is due to

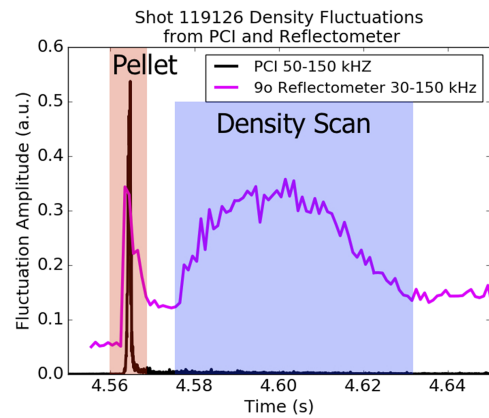


FIG. 7. Time history of density fluctuations measured by PCI (50-150 kHz) and reflectometry (30-150 kHz). The region highlighted in red shows fluctuation changes associated with the pellet injection. The region highlighted in blue shows fluctuation changes on the reflectometer associated with the subsequent density scan and associated shift in measurement location. These two features are clearly separated temporally.

the change in location of the reflectometer cutoff, instead of a temporal change in fluctuation levels.

This comparison engenders confidence that the fluctuation profiles presented in this section are indeed due to a spatial variation in fluctuation levels and not due to temporal changes in fluctuation levels caused by the pellet injection.

B. Fluctuation profile from 9-O reflectometer

Figure 8 shows the density fluctuation profiles for three different frequency ranges measured by the 9-O reflectometer after a pellet injection. The fluctuation frequencies shown are not adjusted for the Doppler shift and are calculated as in Ref. 23. This figure shows that the fluctuations are strongly peaked near the edge in all frequency ranges, though the lowest frequency range may contain signals from MHD activity, which is not the primary focus of this study.

This profile agrees roughly with some of the PCI inversions in Ref. 22 (for example, the maximum entropy method), which shows a strong peak right near the edge of the plasma,

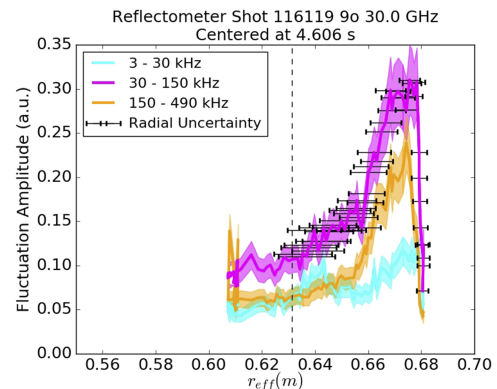


FIG. 8. Density fluctuations measured with the pellet-induced density scan and the 9-O reflectometer in three frequency ranges. The lowest frequency range may contain some signal from MHD events. The vertical dotted line is a_{99} , which is defined as the effective minor radius within which 99% of the total plasma stored energy is confined. Fluctuations are strongly peaked near the plasma edge. Fluctuation uncertainty shown as shaded regions, radial uncertainty as error bars.

TABLE I. The measured full width at half maximum of the density fluctuation profiles near the edge of a series of discharges in LHD.

Shot	Fluctuation FWHM	
	30-150 kHz (cm) \pm 0.25 cm	150-490 kHz (cm) \pm 0.25 cm
116 119	1.81	1.52
119 128	2.32	1.41
119 129	2.02	1.55
119 130	2.09	1.25
119 131	2.04	1.09
119 132	2.37	1.53
119 133	1.07	1.38

while disagreeing significantly with other inversions (for example, the auto-regressive method). In addition, this profile agrees generally with the edge peaking seen in tokamaks. PCI inversions have not yet been completed for this shot, and such comparisons will be the subject of future work.

It must be noted that these two diagnostics measure different turbulent wavenumbers, with reflectometry measuring a specific k up to 15 cm^{-15} and PCI measuring an integrated k -spectrum from 1 to 9 cm^{-1} .²² For this reason, quantitative comparisons of turbulence levels are inappropriate, but qualitative comparisons of the shape and location of the peak of the fluctuation profile are still meaningful. As discussed before, the wide range of profiles that result from different PCI inversion methods motivate an additional method for measuring fluctuation profiles, even if the wavenumber spectrum is slightly different.

In both this shot and others, the radial width of the fluctuation feature seems to be the largest for the 30–150 kHz range (1.5–3 cm full width at half maximum), with a decreasing width at higher frequencies. A summary of the radial width (full width at half maximum) of the fluctuation profile for a series of shots is given in Table I. These shots varied slightly in plasma parameters and were primarily intended to verify that the method of profile measurement described in this paper worked on additional discharges. Further investigation of this turbulent feature width, including parametric scans, will be the subject of future work.

C. Fluctuation profile from comb reflectometer

In addition to the 9-O reflectometer, the edge density fluctuation profile was also measured with the comb channels. As with the velocity measurements, the comb density fluctuation measurements all use arbitrary units, and each channel uses different arbitrary units. The comb reflectometer must therefore be calibrated to the 9-O reflectometer using the same method as was used for the velocity measurements.

Figure 9 shows the calibrated comb measurements. Again, there are three comb channels that were not operating properly in this shot, which are omitted from this figure. While the agreement for the fluctuation profile is not as clean as for the velocity profile, the various channels clearly show a very similar profile shape and location. There is some discrepancy in the inner radii, but this may have to do with the noise floor for the comb channels, which is higher than for the 9-O reflectometer.

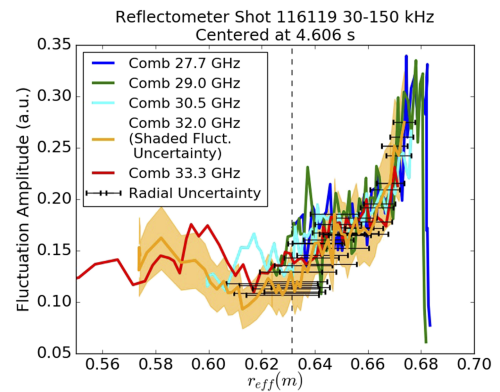


FIG. 9. Density fluctuations in the 30–150 kHz range measured with the pellet-induced density scan and five channels of the comb reflectometer. A cutoff density scaling of 0.75 was used. Calibrated to the 9-O measurement. The vertical dotted line is a_{99} , which is defined as the effective minor radius within which 99% of the total plasma stored energy is confined. Representative uncertainty shown for the 32.0 GHz channel (fluctuation level in shaded orange, radial as black error bars). Once calibrated, most channels agree within error bars.

A more detailed calibration of the comb reflectometer and application to other time periods in the shot, in addition to the pellet injection, will be addressed in future work.

V. CONCLUSIONS

This work has described a new method for measuring density fluctuation profiles in LHD using a pellet-induced density scan and reflectometry. Fast density profiles are measured with 1 ms time resolution using the FIR diagnostic. The cutoff location of the reflectometer is then calculated using a scaled cutoff density, which is matched to the 3D ray tracing code LHD-GAUSS to ensure accuracy. The fast cutoff mapping then enables measurement of velocity and density fluctuation profile via fast density scans caused by pellet injections. Velocity profiles agree qualitatively with CXS results and may agree quantitatively when the k -spectrum and uncertainty in the mapping location are taken into account.

The measured density fluctuation profiles strongly peaked near the edge of the plasma, as is seen on many tokamaks^{6–11} and other helical devices,^{16–18} and in contrast to the results of some inversion methods for PCI on LHD.²² The full width at half maximum of the turbulence layer near the edge is typically only 1.5–3 cm for the discharges considered here, less than 5% of the normalized minor radius.

The results of this study suggest that the limited spatial resolution of PCI (typically 10% to 50% of the normalized minor radius, depending on the inversion method and the spectrum of turbulence wave numbers²²) makes the inversion method critical to determining the correct density fluctuation profile. The method developed here will inform future inversions of PCI measurements, as well as other aspects of PCI measurements, such as up-down asymmetry and systematic offset due to optics.²²

In the future, this technique will be applied to a much larger variety of shots, and proper calibration of the comb channels will enable measurement at times other than the pellet injection itself. Fluctuation profiles measured with PCI

and reflectometry will also be compared from the same shot. Finally, the uncertainty in these measurements will be better quantified. It is also possible that such a technique may be able to inform gyrokinetic simulations of stellarator plasmas.

ACKNOWLEDGMENTS

This work is supported by the US DOE under Grant No. DE-SC0006419 and by the MIT International Science and Technology Internship (MISTI) Program. The authors would also like to thank the technical staff of the Large Helical Device for their support of these experiments. This work is partly supported by a Grant-in-Aid for Scientific Research of the Japan Society for the Promotion of Science (JSPS) (No. 15H02336). This work is also partly supported by the National Institute for Fusion Science grant administrative budget (No. NIFS10ULHH021).

- ¹W. Mandl, R. C. Wolf, M. G. von Hellermann, and H. P. Summers, *Plasma Phys. Controlled Fusion* **35**, 1373 (1993).
- ²H. Weisen, *Infrared Phys.* **25**(3), 543–549 (1985).
- ³M. Hirsch, E. Holzhauser, J. Baldzuhn, B. Kurzan, and B. Scott, *Plasma Phys. Controlled Fusion* **43**, 1641 (2001).
- ⁴G. D. Conway, J. Schirmer, S. Klengel, W. Suttrop, E. Holzhauser, and ASDEX Upgrade Team, *Plasma Phys. Controlled Fusion* **46**, 951 (2004).
- ⁵T. Tokuzawa, A. Ejiri, K. Kawahata, K. Tanaka, I. Yamada, M. Yoshinuma, K. Ida, and C. Suzuki, *Rev. Sci. Instrum.* **83**, 10E322 (2012).
- ⁶G. R. Hanson, J. H. Harris, J. B. Wilgen, C. E. Thomas, S. C. Aceto, L. R. Baylor, J. D. Bell, B. Branas, J. L. Dunlap, and A. C. England, *Nucl. Fusion* **32**, 1593 (1992).
- ⁷R. Sabot *et al.*, *Plasma Phys. Controlled Fusion* **48**, B421–B432 (2006).
- ⁸G. R. McKee, R. J. Fonck, D. K. Gupta, D. J. Schlossberg, M. W. Shafer, R. L. Boivin, and W. Solomon, *Plasma Fusion Res.* **2**, S1025 (2007).
- ⁹Z. Yan, G. R. McKee, R. J. Groebner, P. B. Snyder, T. H. Osborne, and K. H. Burrell, *Phys. Rev. Lett.* **107**, 055004 (2011).
- ¹⁰R. J. Groebner *et al.*, *Nucl. Fusion* **53**, 093024 (2013).
- ¹¹U. Stroth *et al.*, *Nucl. Fusion* **55**, 083027 (2015).
- ¹²M. Kotschenreuther, W. Dorland, M. A. Beer, and G. W. Hammett, *Phys. Plasmas* **2**, 2381 (1995).
- ¹³M. Fujiwara *et al.*, *Nucl. Fusion* **41**(10), 1355 (2001).
- ¹⁴O. Motojima *et al.*, *Nucl. Fusion* **43**, 1674 (2003).
- ¹⁵T. Uckan, C. Hidalgo, J. D. Bell, J. H. Harris, J. L. Dunlap, J. B. Wilgen, Ch. P. Ritz, T. L. Rhodes, and A. J. Wootton, *Phys. Fluids B* **3**, 1000 (1991).
- ¹⁶M. Saffman, S. Zoletnik, N. P. Basse, W. Svendsen, G. Kocsis, and M. Endler, *Rev. Sci. Instrum.* **72**(6), 2579 (2001).
- ¹⁷N. P. Basse, P. K. Michelsen, S. Zoletnik, M. Saffman, M. Endler, and M. Hirsch, *Plasma Sources Sci. Technol.* **11**, A138–A142 (2002).
- ¹⁸T. Happel, “Doppler reflectometry in the TJ-II stellarator: Design of an optimized Doppler reflectometer and its application to turbulence and radial electric field studies,” Ph.D. thesis, Universidad Carlos III de Madrid, 2010.
- ¹⁹K. Tanaka, L. N. Vyacheslavov, T. Akiyama, A. Sanin, K. Kawahata, T. Tokuzawa, Y. Ito, S. Tsuji-Iio, and S. Okajima, *Rev. Sci. Instrum.* **74**(3), 1633 (2003).
- ²⁰K. Tanaka, C. A. Michael, L. N. Vyacheslavov, A. L. Sanin, K. Kawahata, T. Akiyama, T. Tokuzawa, and S. Okajima, *Rev. Sci. Instrum.* **79**, 10E702 (2008).
- ²¹C. A. Michael, K. Tanaka, L. N. Vyacheslavov, A. Sanin, N. Karchev, T. Akiyama, K. Kawahata, and S. Okajima, *Plasma Fusion Res.* **3**, S1071 (2008).
- ²²C. A. Michael, K. Tanaka, L. Vyacheslavov, A. Sanin, and K. Kawahata, *Rev. Sci. Instrum.* **86**, 093503 (2015).
- ²³T. Tokuzawa, A. Ejiri, and K. Kawahata, *Rev. Sci. Instrum.* **81**, 10D906 (2010).
- ²⁴T. Tokuzawa *et al.*, *Plasma Fusion Res.* **9**, 1402149 (2014).
- ²⁵S. Kubo *et al.*, *AIP Conf. Proc.* **669**, 187 (2003).
- ²⁶T. Li Tsujimura *et al.*, *Nucl. Fusion* **55**, 123019 (2015).
- ²⁷C. Suzuki, K. Ida, Y. Suzuki, M. Yoshida, M. Emoto, and M. Yokoyama, *Plasma Phys. Controlled Fusion* **55**, 014016 (2013).
- ²⁸I. Yamada *et al.*, *JINST* **7**, C05007 (2012).
- ²⁹K. Kawahata, A. Ejiri, K. Tanaka, Y. Ito, and S. Okajima, *Fusion Eng. Des.* **34**, 393 (1997).
- ³⁰K. Ida, S. Kado, and Y. Liang, *Rev. Sci. Instrum.* **71**(6), 2360 (2000).
- ³¹M. Yoshinuma, K. Ida, M. Yokoyama, M. Osakabe, and K. Nagaoka, *Fusion Sci. Technol.* **58**, 375 (2010), available at http://www.ans.org/pubs/journals/fst/a_10823.